

1 **Characterization of secondary organic aerosol from heated-** 2 **cooking oil emissions: evolution in composition and volatility**

3 Manpreet Takhar¹, Yunchun Li², Arthur W. H. Chan¹

4 ¹Department of Chemical Engineering and Applied Chemistry, University of Toronto, Toronto, M5S 3E5, Canada

5 ²College of Science, Sichuan Agricultural University, Ya'an, 625014, China

6 *Correspondence to:* Arthur W. H. Chan (arthurwh.chan@utoronto.ca)

7 **Abstract.** Cooking emissions account for a major fraction of urban organic aerosol. It is therefore important to
8 understand the atmospheric evolution in the physical and chemical properties of organic compounds emitted from
9 cooking activities. In this work, we investigate the formation of secondary organic aerosol (SOA) from oxidation of
10 gas-phase organic compounds from heated cooking oil. The chemical composition of cooking SOA is analyzed using
11 thermal desorption-gas chromatography-mass spectrometry (TD-GC/MS). While the particle-phase composition of
12 SOA is a highly complex mixture, we adopt a new method to achieve molecular speciation of the SOA. All the GC
13 elutable material is classified by the constituent functional groups, allowing us to provide a molecular description of
14 its chemical evolution upon oxidative aging. Our results demonstrate an increase in average oxidation state (from -0.6
15 to -0.24), and decrease in average carbon number (from 5.2 to 4.9) with increasing photochemical aging of cooking
16 oil, suggesting that fragmentation reactions are key processes in the oxidative aging of cooking emissions within 2
17 days equivalent of ambient oxidant exposure. Moreover, we estimate that aldehyde precursors from cooking emissions
18 account for a majority of the SOA formation and oxidation products. Overall, our results provide insights into the
19 atmospheric evolution of cooking SOA, a majority of which is derived from gas-phase oxidation of aldehydes.

21 **1 Introduction**

22 Organic aerosol (OA) has important impacts on air quality, climate and human health (Hallquist et al., 2009). OA is
23 often composed of thousands of organic compounds formed from a variety of sources. In urban areas, particulate
24 emissions from food cooking account for a significant fraction of OA (Allan et al., 2010; Crippa et al., 2013; Florou
25 et al., 2017; Kostenidou et al., 2015; Lee et al., 2015; Mohr et al., 2012; Sun et al., 2011). Furthermore, volatile organic
26 compounds (VOCs) are also emitted, and they can undergo oxidation and form secondary organic aerosol (SOA).
27 Recent studies have reported the formation of SOA from meat charbroiling (Kaltsonoudis et al., 2017) and heated
28 cooking oils (Liu et al., 2017b, 2017c, 2018). Therefore, food cooking activities have substantial impacts on air quality
29 in and downwind of urban areas.

30 The emission of VOCs from cooking is highly variable and depends on a number of factors such as cooking style,
31 food, ingredients, and temperature (Fullana et al., 2004a, 2004b; Klein et al., 2016a, 2016b; Liu et al., 2017c; Schauer
32 et al., 1999, 2002). Of the different classes of VOCs characterized in these studies, aldehydes have been shown to be

33 the major group of VOCs emitted from cooking oils. These VOCs are chemically produced upon heating via peroxy
34 radical reactions of the fatty acids (Choe and Min, 2007; Gardner, 1989). Klein et al. (2016a) investigated the
35 composition of nonmethane organic gas (NMOG) emissions from boiling, charbroiling, shallow and deep frying of
36 various vegetables, meats, and cooking oils heated under different temperature conditions. The authors reported that
37 emissions from shallow frying, deep frying and charbroiling are dominated by aldehydes, and the relative amounts
38 depend on the type of oil used during cooking (Klein et al., 2016a). C7 aldehydes are the major species in emissions
39 from canola oil, whereas C9 aldehydes are dominant from olive oil (Klein et al., 2016a). These differences in emission
40 patterns of oils vary with composition of triglycerides present in the oil (Choe and Min, 2006). Katragadda et al.
41 (2010) demonstrated up to an order of magnitude increase in emissions upon reaching the smoke point of cooking
42 oils. In addition to emissions from cooking oil, the addition of condiments (herbs and peppers) to cooking leads to
43 significant emissions of mono-, sesqui- and diterpenes in the gas phase (Klein et al., 2016b). Liu et al. (2017a) showed
44 an order of magnitude increase in the emissions of VOCs when stir-frying with spices. Therefore, factors like cooking
45 style, food, cooking temperature, and ingredients play a significant role in the chemical profile of cooking emissions
46 (Fullana et al., 2004a, 2004b; Klein et al., 2016a, 2016b; Liu et al., 2017a, 2017c).

47 The VOCs emitted from cooking have been shown to produce significant amount of SOA rapidly in recent flow tube
48 (Liu et al., 2017b) and smog chamber studies (Kaltsonoudis et al., 2017; Liu et al., 2017c, 2018). Kaltsonoudis et al.
49 (2017) and Liu et al. (2017b, 2018) showed an increase in O/C ratio upon a few hours of atmospheric aging suggesting
50 lightly oxidized cooking SOA. Furthermore, Liu et al. (2017b) showed significant production of SOA with increasing
51 OH exposure for different cooking oils. Thus far studies have only focused on formation potential of SOA from
52 cooking emissions. Despite high emission rates of VOCs from cooking, the understanding of SOA composition from
53 these emissions remains limited.

54 Source apportionment using aerosol mass spectrometry (AMS) data in urban areas has often revealed a Cooking
55 Organic Aerosol (COA) factor, but it is unclear how this factor is related to cooking emissions. Many studies reported
56 that the mass spectra associated with this factor resemble that of hydrocarbon-like organic aerosol (HOA) factor from
57 other non-cooking sources (Dall'Osto et al., 2015; Hayes et al., 2013; Huang et al., 2010; Mohr et al., 2009, 2012). In
58 addition, it is often unclear whether ambient COA represents primary or secondary organic aerosol from cooking
59 emissions (Dall'Osto et al., 2015; Florou et al., 2017; Kaltsonoudis et al., 2017; Kostenidou et al., 2015). Laboratory
60 studies (Liu et al., 2017b, 2018) showed that the mass spectra for primary cooking organic aerosol exhibited strong
61 correlation with ambient COA factor (Lee et al., 2015), but the cooking SOA mass spectra showed some similarities
62 to ambient semi-volatile oxygenated OA (SV-OOA) factor. These measurements highlight the challenges in assigning
63 COA factor without understanding the changes in chemical composition occurring during oxidation of cooking
64 emissions.

65 In general, there is a need to better understand the molecular composition contributing to aged COA. In this study, we
66 investigate detailed chemical composition of cooking SOA at the molecular level. The objectives of this study are to:
67 (i) understand the detailed chemical speciation of cooking SOA using TD-GC/MS, (ii) describe chemical evolution in
68 SOA upon atmospheric aging, and (iii) attribute formation of SOA to different VOCs emitted from food cooking

69 emissions. In this work we use heated cooking oil as a model for food cooking emissions. We show that the majority
70 of the SOA is derived from oxidation of aldehydes, and the oxidation mechanisms are dominated by fragmentation
71 reactions. Overall, our results provide useful insights into the evolution of cooking SOA, which may be incorporated
72 into chemical transport models for better predicting OA formation from cooking emissions in the atmosphere.

73

74 **2 Experimental methods**

75 **2.1 Flow tube experiments**

76 The experimental setup is shown in Fig. 1, and experimental conditions are listed in Table S1. For each experiment,
77 30-40 mL of canola oil was heated at 250 °C on an electric heating plate in a Pyrex bottle resulting in an average
78 cooking oil temperature of 180 °C, as measured by a thermocouple in direct contact with the heated oil. Purified air
79 flowed over the headspace of the heated oil at a rate of 0.2 L min⁻¹ and then diluted by a factor of 50. 0.2 L min⁻¹ of
80 the total diluted flow was passed through a Teflon filter to remove particles, and the oil vapors were introduced into a
81 custom-built 10 L quartz flow tube reactor. A separate flow of oxygen (99.6%) was irradiated in a UV ozone generator
82 (UVP 97006601) to produce ozone and was also introduced into the flow tube reactor. In parallel, purified air was
83 flowed through a water bubbler into the reactor to provide water vapor. The combined flow rate through the flow tube
84 was set at 3 L min⁻¹, resulting in an average residence time of approximately 200 s.

85 In the flow tube, hydroxyl radicals were produced through the photolysis of ozone irradiated by a UV lamp ($\lambda = 254$
86 nm) in the presence of water vapor. The integrated OH exposure was measured indirectly from the loss of cyclopentane
87 which was monitored by a gas chromatography-flame ionization detector (GC-FID, model 8610C, SRI Instruments
88 Inc.) equipped with a Tenax TA trap sampling downstream of the flow tube at a rate of 0.15 L min⁻¹. In this study, the
89 experiments were conducted at different OH exposures ranging from 5.77×10^{10} to 2.2×10^{11} molecules cm⁻³ s. OH
90 exposure in this range is equivalent to ~11 to 41 h of atmospheric oxidation, respectively, assuming a 24-h average
91 atmospheric OH concentration of 1.5×10^6 molecules cm⁻³ (Mao et al., 2009). The effect of ozone on the SOA
92 formation was found to be negligible as the reaction timescales of aldehydes with ozone were calculated to be at least
93 100 times longer than those with OH. A sample calculation for methacrolein reaction timescales with OH and ozone
94 is shown in SI in Sect. 1.

95 Downstream of the flow tube, pre-baked quartz fiber filter and Tenax tube samples were collected for offline chemical
96 analysis. The changes in the particle size distribution and volume concentration were monitored using a scanning
97 mobility particle sizer (SMPS) with a differential mobility analyzer (TSI 3081), and a condensation particle counter
98 (TSI 3781). A constant density of 1.4 g cm⁻³ was assumed to convert particle volume concentration into mass
99 concentration (Chan et al., 2010). Relative humidity and temperature were monitored by an Omega HX94C RH/T
100 transmitter and were maintained at 65-70%, and 19-20 °C, respectively for all experiments. A fast stepping/scanning
101 thermodenuder (TD, Aerodyne Inc. Billerica, USA) was also placed downstream of the flow tube to measure SOA
102 evaporation rates. Details about TD operating conditions and analysis can be found in Takhar et al. (2019). The TD

103 was only operated during one experiment in which the OH exposure was 9.23×10^{10} molecules cm^{-3} s. The SOA was
104 systematically heated in a TD from 25 °C to 175 °C, and changes in particle volume concentrations and corresponding
105 mass fraction remaining (MFR) were measured using a SMPS. The SOA size distribution during TD operation and
106 volatility distribution are shown in Fig. S1 and S2, respectively. A kinetic mass transfer model developed by Riipinen
107 et al. (2010) was used to interpret the TD data. The inputs to the model are volatility distribution of OA, enthalpy of
108 vaporization, mass accommodation coefficients. Compound groups are translated into volatility distributions by
109 binning components according to their saturation concentrations (Donahue et al., 2006). Parameterization for enthalpy
110 of vaporization was similar to that of Takhar et al. (2019). We assume a surface tension of 0.05 N m^{-1} , gas-phase
111 diffusion coefficients of $5 \times 10^{-6} \text{ m}^2 \text{ s}^{-1}$ for all simulations similar to that reported in Riipinen et al. (2010).

112

113 2.2 Chemical characterization of SOA

114 Tenax tube and quartz filter samples were analyzed separately by thermal desorption gas chromatography mass
115 spectrometry (TD-GC/MS) for detailed chemical speciation of gas- and particle-phase organic compounds. The
116 analyses were performed using a thermal desorption system (TDS 3, Gerstel) combined with a gas chromatography
117 (7890B, Agilent)-mass spectrometer (5977A, Agilent). For gas-phase analysis, concentrations of aldehydes (C7 to
118 C10 *n*-alkanals, alkenals and alkadienals) collected on Tenax tube samples before photooxidation (downstream of the
119 flow tube, with lights off) were quantified. For particle-phase analysis, thermal desorption of quartz filters was
120 performed with *in situ* derivatization using *N*-trimethylsilyl-*N*-methyl trifluoroacetamide (MSTFA). A known amount
121 of deuterated 3-hydroxy-1,5-pentanedioic-2,2,3,4,4- d_5 acid, and *n*-pentadecane- d_{32} (CDN isotopes) was injected,
122 respectively, onto quartz filter punches, and Tenax tubes as internal standards before the samples were desorbed in
123 the TDS. All GC/MS analysis was performed using a non-polar DB5 column (Rxi-5Sil MS, Restek). Details of the
124 operating parameters (GC column, GC and TDS temperature ramps, MS parameters) can be found in Sect. 2 of SI.

125 With *in situ* derivatization, polar organic compounds react rapidly with MSTFA at elevated temperatures during
126 thermal desorption, and functional groups with acidic hydrogen atoms (such as –OH) are replaced by a less polar
127 trimethylsilyl (TMS, [–OSi(CH₃)₃]) group. This reduction in polarity allows the derivatized analyte to elute from a
128 non-polar column and analyzed by subsequent electron impact (EI) at 70 eV. Derivatized compounds produce a
129 signature fragment ion at mass-to-charge (m/z) 73 (–Si(CH₃)₃⁺) arising from the scission of O-Si bond in R-O-
130 [Si(CH₃)₃]. In other words, all derivatized compounds produce ions with m/z 73 during analysis. Therefore, the total
131 signal at m/z 73 can be taken as the total concentration of organic compounds with at least one hydroxyl group
132 (including both –OH and –C(O)OH) present in cooking SOA, much like how m/z 57 represents total concentration of
133 aliphatic compounds in hydrocarbon mixtures (Zhao et al., 2014, 2015). It should be noted that organic peroxides (R-
134 OOH) were also found to be derivatized, but the major reaction product formed is R-O-[Si(CH₃)₃] (which is also
135 formed from R–OH derivatization) as shown in Fig. S3. Here we assume alcohols and acids are the major components,
136 but will explore the potential role of ROOH on the overall chemical composition in Sect. 3.1.

137 As shown in Fig. 2, many compounds in cooking SOA contain at least one –OH group and the chromatogram of m/z
 138 73 is typical of that for a highly complex mixture or unresolved complex mixture (UCM). Using traditional analytical
 139 techniques like GC/MS it is difficult to deconvolute the UCM. However, knowledge about mass spectral
 140 fragmentation of TMS derivatives can be used to understand the compounds contributing to the UCM. Table S2 shows
 141 a list of compounds containing multiple functional groups e.g. –COOH, –OH resulting in different combinations of
 142 compound classes like dicarboxylic acids, hydroxy acids, hydroxy dicarboxylic acids, and dihydroxy dicarboxylic
 143 acids with different carbon numbers. As mentioned earlier, we acknowledge the potential contribution from ROOH,
 144 but will first assume the functional groups shown in Table S2 here, and consider ROOH in more detail in a later
 145 section. The compound groups shown in Table S2 are expected to be formed from oxidation of aldehydes and be
 146 derivatized by MSTFA. The TMS derivatives of these compounds share common ion fragments in their EI mass
 147 spectra: m/z 73 $[\text{Si}(\text{CH}_3)_3]^+$, 75, 147 $[(\text{CH}_3)_2\text{Si}=\text{O}(\text{CH}_3)_3]^+$, M-15 $[\text{M}-\text{CH}_3]^+$ (Jaoui et al., 2004, 2005; Yu et al., 1998).
 148 Most importantly, all TMS derivatives exhibit quantifiable peaks at m/z 73 (ubiquitous ion for all derivatives) and M-
 149 15 (ion specific to each compound group, hereby referred to as the pseudo-parent ion). We also obtained the
 150 characteristic ratio of these two ions for each compound group ($f_{M-15/73}$) from NIST mass spectral libraries and from
 151 analyzing authentic standards. To verify the validity of this method, we calculate the total m/z 73 ion signal that is
 152 attributable to these compound groups by taking the chromatograms of the pseudo-parent ion for each compound
 153 group, dividing by its characteristic ratio $f_{M-15/73}$ and then summing across all compound groups as shown in Eq.
 154 (1).

$$155 \quad S_{73,t}^{sum} = \sum_i \frac{S_{M-15,i,t}}{f_{M-15/73,i}} \quad (1)$$

156 where $S_{73,t}^{sum}$ is the m/z 73 ion signal at retention time t that is attributable to all compound groups listed in Table S2,
 157 $S_{M-15,i,t}$ is the signal of the pseudo-parent ion for compound group i at retention time t , $f_{M-15/73,i}$ is the characteristic
 158 ratio of pseudo-parent ion to m/z 73. This approach is similar to that described in Isaacman-VanWertz et al. (2020).
 159 As shown in Fig. 2, $S_{73,t}^{sum}$ shows excellent agreement with the measured m/z 73 ion signal, suggesting that the m/z 73
 160 signal, which is representative of all TMS derivatives, is almost entirely comprised of contributions from the
 161 compound groups listed in Table S2. This agreement between our bottom-up approach and measured signal provides
 162 confidence that our method is able to provide information about the chemical composition of highly complex mixture.

163 With the signals from all the pseudo parent ions for all compound groups, the total mass of each compound group was
 164 then calculated using Eq. (2).

$$165 \quad M_i = \frac{TA_i}{RF_i} \times \frac{1}{f_{M-15/73,i}} \quad (2)$$

166 where, M_i is the mass of compound group i , TA_i is the total integrated signal of pseudo-parent ion for compound
 167 group i (normalized by the signal of deuterated internal standard), RF is the response factor (calculated from
 168 calibration curves of fatty acids and dicarboxylic acids authentic standards) of compound group i , and $f_{M-15/73,i}$ is
 169 the characteristic ratio of pseudo-parent ion to m/z 73 for compound group i . A more detailed, step-by-step description

170 of the procedure can be found in the SI in Sect. 3, and illustrated in Fig. S4 with corresponding uncertainties in the
171 fitting procedure shown in Fig. S5.

172

173 3 Results and discussion

174 3.1 Chemical evolution of SOA

175 As described in Sect. 2.2, components in cooking SOA were classified by functional groups and carbon number. To
176 describe the overall changes in SOA composition with increasing OH exposure, we use the average carbon oxidation
177 state ($\overline{\text{OSc}}$) as a metric for the evolving composition of a complex mixture undergoing oxidation (Kroll et al., 2011).
178 Both $\overline{\text{OSc}}$ and number of carbon atoms (nc) for each compound group are calculated from the GC-derived chemical
179 composition. The total mole fraction of C, H and O was calculated for each sample which was then used to calculate
180 the bulk $\overline{\text{OSc}}$ using the Eq. $2 \times O:C - H:C$ (Kroll et al., 2011). The evolution in this framework for canola oil SOA
181 is shown in Fig. 3. The bulk $\overline{\text{OSc}}$ was observed to increase from -0.6 to -0.24 when OH exposure increased from 5.77
182 to 22.0×10^{10} molecules cm^{-3} s for canola oil SOA. For comparison, Liu et al. (2017b) showed an initial decrease in
183 $\overline{\text{OSc}}$ and O:C, but gradually stabilized at OH exposure greater than 9×10^{10} molecules cm^{-3} s. For the $\overline{\text{OSc}}$ range reported
184 here, the $\overline{\text{OSc}}$ of cooking SOA falls in the range of SV-OOA as determined from factor analysis of AMS data
185 (Canagaratna et al., 2015). This degree of oxygenation is greater than that of the COA factor measured by AMS, which
186 is reported to be around -1.37 (Canagaratna et al., 2015). This difference suggests that the COA factor resolved using
187 PMF analysis is likely of primary origin and does not represent SOA formed from atmospheric oxidation of cooking
188 emissions. Furthermore, previous GC/MS analysis showed for POA from cooking oils, an $\overline{\text{OSc}}$ of -1.66 (canola oil)
189 and -1.7 (beef tallow, olive oil) was calculated (Takhar et al., 2019). These observations again suggest that COA factor
190 measured by AMS is derived of primary cooking emissions.

191 In addition to carbon oxidation state, knowledge about molecular composition provides further insights into the
192 oxidation mechanisms. Canola oil SOA at an OH exposure of 5.77×10^{10} molecules cm^{-3} s is comprised of ~19%
193 larger (C8-C10) and less oxygenated compounds, this fraction declined to ~11% at higher OH exposures. Furthermore,
194 the total fraction of C2-C7 products increased from 81% to 89% when OH exposure increased from 10.7 h to 1.7 d.
195 Of this fraction, the smaller carbon # compounds (C2-C4) which are indicative of fragmentation processes increased
196 from 42% at 10.7 h to ~49% at 1.7 d. An increase in smaller and more oxygenated compounds, along with decrease
197 in larger and less oxygenated products suggests that fragmentation reactions are responsible for the shift towards
198 formation of smaller oxygenated compounds. As a result, oxidation simultaneously leads to higher $\overline{\text{OSc}}$ and lower
199 carbon number on average. Based on the compounds observable by our technique, this trend suggests that
200 fragmentation reactions are key processes in the oxidative evolution of cooking emissions.

201 The compounds observed here can also be compared to previously measured bulk composition using elemental ratios,
202 such as those presented in a Van Krevelen (VK) diagram (Heald et al., 2010). As shown in Fig. 4, the O:C ratio in our

203 study ranged between 0.64 and 0.79 when OH exposure increased from 5.77×10^{10} to 22.0×10^{10} molecules cm^{-3} s. The
204 O:C ratios measured using an AMS (Kaltsonoudis et al., 2017; Liu et al., 2017b) ranged between 0.24-0.46 which are
205 within a factor of 2 measured in this study. Furthermore, the H:C versus O:C trend is linear with a slope of -0.19,
206 which lies between the slope of 0 measured for low- NO_x oxidation reported by Liu et al. (2017b) and -0.4 for high-
207 NO_x conditions (Liu et al., 2018). Therefore, based on elemental ratios, the evolution in SOA composition measured
208 in this study is comparable to that in bulk average properties estimated by AMS. Furthermore, we use 2D-VBS
209 framework developed by Donahue et al. (2012) to investigate OA chemistry, and understand the evolution of cooking
210 SOA through changes in the volatility of SOA system. The vapor pressures of the identified compounds are calculated
211 using group contribution method (Pankow and Asher, 2008) where experimentally determined vapor pressures were
212 unavailable, and reported in Table S2. The observed compounds in SOA have a broad range of volatilities, since they
213 were formed from oxidation of a complex ensemble of VOC precursors. As shown in Fig. S6, there is minor decrease
214 in overall volatility of the mixture (change lies within one decade in C^*) irrespective of the presence of peroxides,
215 while $\overline{\text{OSc}}$ is increasing with oxidation. This increase in oxidation state is coincident with increasing fragmentation
216 upon oxidation, and, as a result, the overall change in the bulk volatility of canola oil SOA is relatively small.

217 As mentioned earlier in Sect. 2.2, there is a potential to misclassify ROOH as ROH using our current GC/MS method.
218 Here we further examine the chemical composition by assuming that each $-\text{O}[\text{Si}(\text{CH}_3)_3]$ group observed originates
219 from an $-\text{OOH}$ group in the SOA, and to support this argument we show that derivatization of cumene hydroperoxide
220 (Sigma Aldrich Co.) is observed as TMS of hydroxy-cumene in our system as shown in Fig. S3. It should be noted
221 that replacing $-\text{OH}$ with $-\text{OOH}$ results in a higher estimate of O:C (and $\overline{\text{OSc}}$) but does not change H:C or carbon #.
222 Furthermore, since pseudo molecular ion fraction ($f_{M-15/73}$) for organic peroxides (needed for quantification) is
223 unknown, we assume that it is similar to those presented in Table S2. As shown in Fig. S7, if all observed $-\text{OH}$ groups
224 are $-\text{OOH}$ groups, the VK-slope is -0.15 which is similar to -0.19 calculated based on the no-peroxide assumption.
225 Similarly, Fig. S6 shows that this uncertainty in hydroxyl group identification has negligible effect on estimation of
226 vapor pressure or volatility in the 2D-VBS framework. Therefore, this potential misclassification of peroxide groups
227 may lead to an underestimation in O:C and $\overline{\text{OSc}}$, but is not expected to affect estimates of volatility and our general
228 conclusions about the importance of fragmentation reactions. In the future, analytical techniques such as extractive
229 electrospray ionization time-of-flight mass spectrometry (Lopez-Hilfiker et al., 2019) may be useful to better
230 understand the composition of peroxides from cooking SOA. While the misclassification of peroxides may have little
231 impact on the bulk properties such as average O:C ratios, there may be important implications on understanding the
232 reactivity of the SOA.

233

234 3.2 Evaporation rates of SOA

235 The volatility of the SOA is also probed by measuring the evaporation rates in a heated thermodenuder and compared
236 to the rates expected from the measured composition. In order to derive the evaporation rates from the measured
237 chemical composition of cooking SOA, we use the kinetic mass transfer model developed by Riipinen et al. (2010).

238 Among the inputs into the model, the mass accommodation coefficient is a critical but uncertain parameter that
239 accounts for the mass transfer limitations in the system.

240 Figure 5 shows both measured and modeled mass thermograms for canola oil SOA. We observe that for canola oil
241 SOA, mass accommodation coefficient of 0.03 is needed to predict the experimentally determined mass thermograms.
242 An accommodation coefficient of <1 suggests that mass transfer limitations in the system likely occurring in the
243 condensed-phase. Formation of multifunctional organic compounds such as those observed in this study is likely
244 responsible for an increase in viscosity through increasing hydrogen bonding and other polar interactions (Rothfuss
245 and Petters, 2016). It should be noted that Takhar et al. (2019) reported similar magnitudes of mass accommodation
246 coefficients for heterogeneous oxidation of cooking oil particles. Due to similarity in the type of functional groups
247 present in both aging pathways, we believe the decrease in mass accommodation coefficients for both systems undergo
248 similar changes in phase and/or viscosity.

249 These measurements of evaporation rates are consistent with the volatilities expected from our measured composition
250 of SOA containing small oxygenated compounds. Although mass accommodation coefficients are highly uncertain,
251 the mass accommodation coefficients for other SOA systems have been measured to be even lower on the order of 10^{-4}
252 (Cappa and Wilson, 2011), which would require the volatilities to be even higher to explain the measured evaporation
253 rates. Therefore, the TD measurements support the conclusion that smaller oxygenated compounds are produced from
254 oxidation of cooking oil vapors, and that fragmentation reactions are dominant. Furthermore, these measurements
255 provide useful inputs into chemical transport models for predicting SOA formation and gas-particle partitioning. Our
256 previous work (Takhar et al., 2019) showed that even at $\alpha = 10^{-2}$, gas-particle partitioning timescales are short (within
257 hours) and the assumption of equilibrium partitioning still holds for regional scale SOA formation. Further work is
258 needed to directly measure the viscosity of cooking SOA, and corresponding mixing timescales to better constrain the
259 physicochemical properties of cooking SOA.

260

261 **3.3 Contribution of aldehydes to observed oxidation products and total SOA**

262 Since cooking oil vapors are comprised of a number of reactive aldehydes that can lead to SOA formation, we conduct
263 further experiments of SOA formation from these precursors and identify the relative contributions to observed
264 oxidation products and to total SOA. These results are applied to the heated cooking oil experiments to understand the
265 role of aldehydes in the overall production and evolution of cooking oil SOA.

266 **3.3.1 Formation of particle-phase oxidation products**

267 As described in the earlier sections, we are able to quantify the mass concentrations of different compound groups (6
268 different combinations of functional groups, from C2 to C10, summarized in Table S2) in the particle phase for all
269 experiments. We denote the observed mass concentrations of compound group i in SOA from canola oil
270 photooxidation as M_i^{oil} . The expected precursors to these oxidation products are likely aldehydes, since aldehydes are

271 emitted in significant amounts and are highly reactive. To examine this hypothesis, here we calculate the formation
272 of these observed compound groups from oxidation of aldehydes. For this calculation, heptanal, *trans*-2-heptenal,
273 *trans*-2-octenal, *trans,trans*-2,4-heptadienal, and *trans,trans*-2,4-decadienal (Sigma Aldrich Co.) were considered
274 because these aldehydes are the dominant VOC precursors emitted from heated canola oil in our experiments as shown
275 in Fig. S8. More volatile aldehydes, such as acrolein and methacrolein, were likely present but could not be captured
276 and analyzed by our techniques. The molar amount reacted for each aldehyde j in the canola oil oxidation experiments
277 is denoted as ΔVOC_j^{oil} , and was calculated based on the measured OH exposure.

278 In order to estimate the contribution from oxidation of an aldehyde j in the gas-phase mix to the formation of each
279 compound group i , we conducted a series of experiments in which a representative aldehyde was oxidized, and the
280 molar yields of the various compounds were measured:

$$281 \quad \gamma_{ij} = \frac{M_{ij}^{ind}/MW_i}{\Delta VOC_j^{ind}} \quad (3)$$

282 where γ_{ij} represents the molar yield of compound group i from precursor j , M_{ij}^{ind} denotes the mass concentration of
283 compound i observed in photooxidation experiments in which aldehyde j was the sole precursor, MW_i is the molecular
284 weight of compound i , and ΔVOC_j^{ind} is the amount of precursor j reacted in each experiment. γ_{ij} is then applied to the
285 heated cooking oil experiments to estimate the amount of oxidation products that would form from each precursor:

$$286 \quad M_i^{sum} = \sum_j \gamma_{ij} \Delta VOC_j^{oil} MW_i \quad (4)$$

287 A sample calculation for this analysis is presented in Sect. 4 of SI. The comparison between M_i^{sum} (contribution of
288 aldehyde oxidation to formation of compound i) and M_i^{oil} (observed concentrations of compound i) is shown in Fig.
289 6. Based on this methodology, oxidation of aldehydes accounts for $63 \mu\text{g m}^{-3}$ (M_i^{sum}) of the observed $75 \mu\text{g m}^{-3}$ (M_i^{oil})
290 (or 84%) particle-phase oxidation products measured at an OH exposure of 6.43×10^{10} molecules cm^{-3} s. The
291 contributions of alkanals (heptanal), alkenals (heptenal + octenal) and alkadienals (heptadienal + decadienal) are 7%,
292 ~31% and 46%, respectively.

293 While the amount of oxidation products expected from aldehydes is somewhat lower than that observed in canola oil
294 SOA, this difference may arise from differences in gas-particle partitioning between single aldehyde photooxidation
295 and canola oil photooxidation. As shown in Fig. 6, the formation of higher carbon # products cannot be explained
296 from the photooxidation of aldehydes used to predict oil oxidation products likely due to the assumption of negligible
297 particle-phase or oligomerization reactions occurring in the condensed phase. In addition, higher carbon # acids are
298 likely present as primary vapors in the gas phase which can then partition to the condensed phase upon SOA formation.
299 As shown in Fig. S9, more oxygenated compounds (higher O:C and greater number of functional groups) tend to be
300 more abundant in the canola oil SOA than expected from aldehyde photooxidation, suggesting that canola oil SOA is
301 more favorable for oxygenated compounds to partition than SOA from individual aldehydes. On the other hand, there
302 is no clear trend in partitioning with respect to vapor pressures and carbon number. It should be noted that uncertainties

303 in the fitting procedure or estimation in the pseudo molecular ion (refer to Table S2 and Fig. S5) can also result in
304 uncertainties between -40% and +20%. Therefore, in summary, the quantified oxidation products from canola oil SOA
305 are generally consistent with those from aldehyde photooxidation, and the relative amounts may be subject to further
306 changes due to gas-particle partitioning.

307

308 3.3.2 Using the statistical oxidation model (SOM) framework

309 To further explore the evolution of canola oil SOA, we applied our results to the statistical oxidation model (SOM)
310 framework developed by Cappa and Wilson (Cappa et al., 2013; Cappa and Wilson, 2012). SOM describes the
311 oxidation chemistry of a VOC precursor through multi-generational space defined by the number of carbon and
312 oxygen atoms present in the precursor and its possible SOA product molecules. The SOM does not specifically track
313 the product composition in terms of functional groups, but provides adequate details to represent key atmospheric
314 processes such as gas-particle partitioning, fragmentation, functionalization, reactions with oxidants, condensed-phase
315 chemistry. The model has been applied to chamber experiments to derive parametrizations by fitting experimental
316 data to both SOA mass concentration and the bulk aerosol O/C ratio. Eluri et al. (2018) used the chamber derived
317 parameterizations to predict the properties of SOA generated from diesel exhaust in an oxidation flow tube reactor.

318 To the best of the authors' knowledge, there are no parameterizations for the oxidation of aldehydes. Therefore, in
319 this study we first derived the parameterizations for aldehyde oxidation, and then use these parameters to predict the
320 SOA mass concentrations. In order to obtain the parameters, we fit the measured SOA concentration from oxidation
321 of heptanal, *trans*-2-heptenal, *trans,trans*-2,4-heptadienal at different OH exposures to optimize the six tunable
322 parameters under low-NO_x conditions (shown in Fig. S10). Best fit SOM parameters indicate that photooxidation
323 leads to fragmentation per reaction with OH, as shown by a lower *mfrag* than compared to other systems e.g. alkanes
324 (≥ 2 for branched, cyclic or *n*-alkane under low-NO_x conditions (Eluri et al., 2018)). Since a lower value for *mfrag*
325 represents greater fragmentation (Cappa and Wilson, 2012), this again reflects the higher propensity for fragmentation
326 in this SOA system. The optimized parameters were then used to predict the SOA concentration for canola oil
327 photooxidation under different aging conditions in the OH exposure range similar to that of aldehyde photooxidation.

328 Based on these established parameterizations for different aldehydes, model simulations were conducted for canola
329 oil having a mixture of aldehydes under different photochemical aging conditions. It should be noted that we used
330 parameterizations of heptanal for all alkanals, heptenal for all alkenals, and heptadienal for alkadienals. As shown in
331 Fig. 7, the model generally captures the amount of SOA formed to up to 62%, but overpredicts SOA formation at
332 lower photochemical ages and underpredicts SOA concentrations at higher photochemical ages. In addition, SOM
333 also tracks atomic O/C ratio which were further compared with the measured O/C ratio. SOM predicts an O:C around
334 0.51, which is within 50% of the measured O:C likely suggesting that the changes in chemical composition of cooking
335 SOA is in a reasonable agreement with the model predictions. Furthermore, the unexplained SOA can likely arise
336 from other unidentified S/IVOCs as hypothesized by Liu et al. (2017c). However, unlike traffic emissions (Zhao et

337 al., 2014), S/IVOCs from cooking has not been positively identified. In addition, small VOC precursors like acrolein
338 and malondialdehyde which have been measured in large quantities from cooking emissions (Klein et al., 2016a), may
339 form SOA products having higher O/C ratios, which may better explain the O/C ratios observed in our experiments.

340 One inconsistency between the model and measurements is the slope at which SOA is being formed. The experimental
341 data suggest a steeper trend of SOA formation while the model predicts a more gradual increase in SOA formation. A
342 potential explanation for this discrepancy is the contribution from other unmeasured VOCs. These VOCs are less
343 reactive than those considered in the model, such that they contribute to higher SOA at higher OH exposures.
344 Alternatively, these missing VOCs are more volatile such that more of their SOA is formed at later generations of
345 oxidation. For example, acrolein forms SOA with measurable yields (Chan et al., 2010) and is emitted at large amounts
346 from heated cooking oils (Klein et al., 2016a). Despite these limitations, these parameterizations generally capture the
347 amount of SOA formed and its degree of oxidation (O/C) on oxidation timescales relevant to urban areas (within 2
348 days) and are useful for representing cooking oil emissions in the chemical transport models. Overall, the amount of
349 SOA formed and the evolution upon oxidation can be well described by photooxidation of aldehydes.

350

351 **4 Conclusions and implications**

352 In this work, we characterized the detailed chemical composition of SOA generated from cooking oil vapors. We
353 showed that cooking SOA occurring as highly complex mixture can be deconvoluted using mass spectral
354 fragmentation pattern to extract useful information about the chemical identities of organic compounds, such as
355 functional groups and carbon number. Using this detailed chemical composition of cooking SOA, we showed that
356 fragmentation is an important pathway for oxidative processing of cooking emissions in the atmosphere even within
357 short timescales of oxidation. Furthermore, we showed that aldehydes can reasonably explain the formation of SOA
358 generated from cooking oil vapors and the oxidative evolution as described using a multi-generational oxidation
359 model. Our study, therefore, highlights the importance of molecular composition in constraining the chemical
360 properties of cooking SOA, as well as understanding the contribution of aldehydes in formation of SOA from cooking
361 emissions.

362 Consistent with other studies, our work has shown that aldehydes are an important class of VOC precursors emitted
363 from cooking emissions, and substantial efforts have been made to measure their emission factors depending on
364 different cooking settings (heating temperature, cooking style, food, ingredients) (Klein et al., 2016a, 2016b).
365 However, the contribution of aldehydes from cooking emissions is underrepresented in chemical transport models.
366 Recently, McDonald et al. (2018) showed that the ambient concentrations of OA were underpredicted when aldehydes
367 were not included in the box model calculations, suggesting that aldehydes, likely from food cooking, play an
368 important role in atmospheric oxidation chemistry. Furthermore, Klein et al. (2019) showed that heavy pollutants like
369 restaurants play a significant role in contributing to the ambient cooking organic aerosol concentrations. In this study,
370 we showed a large fraction of the SOA is derived from aldehyde precursors, with strong similarities in chemical
371 composition. Therefore, it is important to consider the contribution of aldehyde chemistry in atmospheric models

372 towards total OA budget. Furthermore, we demonstrated the importance of fragmentation reactions and their influence
373 on OA properties such as volatility and chemical composition. Future work should therefore focus on measuring not
374 only the SOA formation, but also the oxygenated VOCs formed due to fragmentation upon aging to provide insights
375 into aging of cooking emissions.

376 Formation of SOA from cooking emissions in the atmosphere is likely influenced by emissions of POA, and other
377 gas-phase precursors. Therefore, inclusion of POA during atmospheric processing of cooking emissions will likely
378 influence the physicochemical properties of cooking SOA. For instance, with cooking POA being much less
379 functionalized than SOA, inclusion of POA will likely decrease the system O:C (or $\overline{O:C}$). However, POA from
380 cooking emissions can undergo heterogeneous reactions in the atmosphere, thereby increasing O:C (or $\overline{O:C}$). On the
381 other hand, there could potentially be contributions from other gas-phase precursors or S/IVOCs emitted from cooking
382 vapors that can result in SOA formation. These precursors can potentially contribute to SOA formation from cooking
383 emissions, but their oxidative evolution in the atmosphere is not well understood.

384 Gas-particle partitioning of SOA can be further affected by non-ideal mixing, as well as morphology of the particles
385 (Shiraiwa et al., 2013; Zuend and Seinfeld, 2012). Future work should investigate the effect of these parameters on
386 cooking SOA properties and formation potential. To account for thermodynamic mixing favourability of the particles,
387 Hansen solubility framework developed by Ye et al. (2016) can be implemented to provide insights into SOA mixing
388 and yield enhancement. As shown in Ye et al. (2018) primary meat-cooking emissions can enhance SOA yield from
389 α -pinene due to similarity in Hansen solubility parameters suggesting that primary meat cooking particles are miscible
390 with α -pinene SOA. It should be noted that present study did not investigate the effect of atmospherically relevant
391 seed particles as well as NO_x levels which are representative of typical urban environments. Since emissions upon
392 entering the atmosphere gets mixed with background air, other source emissions, and diluted upon mixing thereby
393 altering the gas-particle partitioning, and thus the total OA loading. Therefore, it is important to understand the changes
394 in partitioning and miscibility of cooking emissions as the composition continually evolves with atmospheric
395 processing. Additionally, as mentioned earlier cooking SOA undergoes large mass transfer limitations due to changes
396 in the phase state of the SOA particles, making it more so important to experimentally determine the corresponding
397 viscosity of cooking SOA. Therefore, future work should focus on measuring both the viscosity and miscibility of
398 SOA derived from cooking emissions.

399

400 *Data availability.* The data are available upon request to the corresponding author.

401

402 *Author Contributions.* MT and AWHC designed research. MT collected and analyzed data. MT, YL and AWHC
403 interpreted results. MT and AWHC wrote the manuscript with inputs from YL.

404

405 *Competing interests.* The authors declare that they have no conflict of interests.

406

407 *Acknowledgements.* The authors acknowledge Environment and Climate Change Canada (ECCC) for funding support
408 through the Government of Canada Grants and Contribution program. The authors would like to thank Shao-Meng Li
409 from ECCC for use of the thermodenuder, Chris Cappa from UC Davis for help with SOM simulations, Greg Evans,
410 Jeff Brook and Tengyu Liu from University of Toronto for helpful discussion.

411 **References**

- 412 Allan, J. D., Williams, P. I., Morgan, W. T., Martin, C. L., Flynn, M. J., Lee, J., Nemitz, E., Phillips, G. J.,
413 Gallagher, M. W. and Coe, H.: Contributions from transport, solid fuel burning and cooking to primary organic
414 aerosols in two UK cities, *Atmos. Chem. Phys.*, 10(2), 647–668, doi:10.5194/acp-10-647-2010, 2010.
- 415 Canagaratna, M. R., Jimenez, J. L., Kroll, J. H., Chen, Q., Kessler, S. H., Massoli, P., Hildebrandt Ruiz, L., Fortner,
416 E., Williams, L. R., Wilson, K. R., Surratt, J. D., Donahue, N. M., Jayne, J. T. and Worsnop, D. R.: Elemental ratio
417 measurements of organic compounds using aerosol mass spectrometry: Characterization, improved calibration, and
418 implications, *Atmos. Chem. Phys.*, 15(1), 253–272, doi:10.5194/acp-15-253-2015, 2015.
- 419 Cappa, C. D. and Wilson, K. R.: Evolution of organic aerosol mass spectra upon heating: Implications for OA phase
420 and partitioning behavior, *Atmos. Chem. Phys.*, 11(5), 1895–1911, doi:10.5194/acp-11-1895-2011, 2011.
- 421 Cappa, C. D. and Wilson, K. R.: Multi-generation gas-phase oxidation, equilibrium partitioning, and the formation
422 and evolution of secondary organic aerosol, *Atmos. Chem. Phys.*, 12(20), 9505–9528, doi:10.5194/acp-12-9505-
423 2012, 2012.
- 424 Cappa, C. D., Zhang, X., Loza, C. L., Craven, J. S., Yee, L. D. and Seinfeld, J. H.: Application of the Statistical
425 Oxidation Model (SOM) to Secondary Organic Aerosol formation from photooxidation of C12 alkanes, *Atmos.*
426 *Chem. Phys.*, 13(3), 1591–1606, doi:10.5194/acp-13-1591-2013, 2013.
- 427 Chan, A. W. H., Chan, M. N., Surratt, J. D., Chhabra, P. S., Loza, C. L., Crouse, J. D., Yee, L. D., Flagan, R. C.,
428 Wennberg, P. O. and Seinfeld, J. H.: Role of aldehyde chemistry and NO_x concentrations in secondary organic
429 aerosol formation, *Atmos. Chem. Phys.*, 10(15), 7169–7188, doi:10.5194/acp-10-7169-2010, 2010.
- 430 Choe, E. and Min, D. B.: Mechanisms and factors for edible oil oxidation, *Compr. Rev. Food Sci. Food Saf.*, 5(4),
431 169–186, doi:10.1111/j.1541-4337.2006.00009.x, 2006.
- 432 Choe, E. and Min, D. B.: Chemistry of deep-fat frying oils, *J. Food Sci.*, 72(5), doi:10.1111/j.1750-
433 3841.2007.00352.x, 2007.
- 434 Crippa, M., Decarlo, P. F., Slowik, J. G., Mohr, C., Heringa, M. F., Chirico, R., Poulain, L., Freutel, F., Sciare, J.,
435 Cozic, J., Di Marco, C. F., Elsasser, M., Nicolas, J. B., Marchand, N., Abidi, E., Wiedensohler, A., Drewnick, F.,
436 Schneider, J., Borrmann, S., Nemitz, E., Zimmermann, R., Jaffrezou, J.-L., Prevot, A. S. H. and Baltensperger, U.:
437 Wintertime aerosol chemical composition and source apportionment of the organic fraction in the metropolitan area
438 of Paris, *Atmos. Chem. Phys.*, 13(2), 961–981, doi:10.5194/acp-13-961-2013, 2013.
- 439 Dall’Osto, M., Paglione, M., Decesari, S., Facchini, M. C., O’Dowd, C., Plass-Duellmer, C. and Harrison, R. M.: On
440 the Origin of AMS “cooking Organic Aerosol” at a Rural Site, *Environ. Sci. Technol.*, 49(24), 13964–13972,
441 doi:10.1021/acs.est.5b02922, 2015.
- 442 Donahue, N. M., Robinson, A. L., Stanier, C. O. and Pandis, S. N.: Coupled partitioning, dilution, and chemical
443 aging of semivolatile organics, *Environ. Sci. Technol.*, 40(8), 2635–2643, doi:10.1021/es052297c, 2006.
- 444 Donahue, N. M., Kroll, J. H., Pandis, S. N. and Robinson, A. L.: A two-dimensional volatility basis set-Part 2:
445 Diagnostics of organic-aerosol evolution, *Atmos. Chem. Phys.*, 12(2), 615–634, doi:10.5194/acp-12-615-2012,
446 2012.
- 447 Eluri, S., Cappa, C. D., Friedman, B., Farmer, D. K. and Jathar, S. H.: Modeling the formation and composition of
448 secondary organic aerosol from diesel exhaust using parameterized and semi-explicit chemistry and thermodynamic
449 models, *Atmos. Chem. Phys.*, 18(19), 13813–13838, doi:10.5194/acp-18-13813-2018, 2018.
- 450 Florou, K., Papanastasiou, D. K., Pikridas, M., Kaltsonoudis, C., Louvaris, E., Gkatzelis, G. I., Patoulias, D.,
451 Mihalopoulos, N. and Pandis, S. N.: The contribution of wood burning and other pollution sources to wintertime
452 organic aerosol levels in two Greek cities, *Atmos. Chem. Phys.*, 17(4), 3145–3163, doi:10.5194/acp-17-3145-2017,
453 2017.

- 454 Fullana, A., Carbonell-Barrachina, A. A. and Sidhu, S.: Comparison of volatile aldehydes present in the cooking
455 fumes of extra virgin olive, olive, and canola oils, *J. Agric. Food Chem.*, 52(16), 5207–5214, doi:10.1021/jf035241f,
456 2004a.
- 457 Fullana, A., Carbonell-Barrachina, A. A. and Sidhu, S.: Volatile aldehyde emissions from heated cooking oils, *J.*
458 *Sci. Food Agric.*, 84(15), 2015–2021, doi:10.1002/jsfa.1904, 2004b.
- 459 Gardner, H. W.: Oxygen radical chemistry of polyunsaturated fatty acids, *Free Radic. Biol. Med.*, 7(1), 65–86,
460 doi:10.1016/0891-5849(89)90102-0, 1989.
- 461 Hallquist, M., Wenger, J. C., Baltensperger, U., Rudich, Y., Simpson, D., Claeys, M., Dommen, J., Donahue, N. M.,
462 George, C., Goldstein, A. H., Hamilton, J. F., Herrmann, H., Hoffmann, T., Iinuma, Y., Jang, M., Jenkin, M. E.,
463 Jimenez, J. L., Kiendler-Scharr, J., Maenhaut, W., McFiggans, G., Mentel, T. F., Monod, A., Prevot, A. S. H.,
464 Seinfeld, J. H., Surratt, J. D., Szmigielski, R. and Wildt, J.: The formation, properties and impact of secondary
465 organic aerosol: current and emerging issues, *Atmos. Chem. Phys.*, 9(14), 5155–5236, doi:10.5194/acp-9-5155-
466 2009, 2009.
- 467 Hayes, P. L., Ortega, A. M., Cubison, M. J., Froyd, K. D., Zhao, Y., Cliff, S. S., Hu, W. W., Toohey, D. W., Flynn,
468 J. H., Lefer, B. L., Grossberg, N., Alvarez, S., Rappenglück, B., Taylor, J. W., Allan, J. D., Holloway, J. S., Gilman,
469 J. B., Kuster, W. C., De Gouw, J. A., Massoli, P., Zhang, X., Liu, J., Weber, R. J., Corrigan, A. L., Russell, L. M.,
470 Isaacman, G., Worton, D. R., Kreisberg, N. M., Goldstein, A. H., Thalman, R., Waxman, E. M., Volkamer, R., Lin,
471 Y. H., Surratt, J. D., Kleindienst, T. E., Offenberg, J. H., Dusanter, S., Griffith, S., Stevens, P. S., Brioude, J.,
472 Angevine, W. M. and Jimenez, J. L.: Organic aerosol composition and sources in Pasadena, California, during the
473 2010 CalNex campaign, *J. Geophys. Res. Atmos.*, 118(16), 9233–9257, doi:10.1002/jgrd.50530, 2013.
- 474 Heald, C. L., Kroll, J. H., Jimenez, J. L., Docherty, K. S., Decarlo, P. F., Aiken, A. C., Chen, Q., Martin, S. T.,
475 Farmer, D. K. and Artaxo, P.: A simplified description of the evolution of organic aerosol composition in the
476 atmosphere, *Geophys. Res. Lett.*, 37(8), doi:10.1029/2010GL042737, 2010.
- 477 Huang, X., He, L., Hu, M., Canagaratna, M. R., Sun, Y., Zhang, Q., Zhu, T., Xue, L., Zeng, L. W., Liu, X. G.,
478 Zhang, Y. H., Jayne, J. T., Ng, N. L. and Worsnop, D. R.: and Physics Highly time-resolved chemical
479 characterization of atmospheric submicron particles during 2008 Beijing Olympic Games using an Aerodyne High-
480 Resolution Aerosol Mass Spectrometer, *Atmos. Chem. Phys.*, 10(18), 8933–8945, doi:10.5194/acp-10-8933-2010,
481 2010.
- 482 Isaacman-VanWertz, G., Lu, X., Weiner, E., Smiley, E. B. and Widdowson, M. A.: Characterization of hydrocarbon
483 groups in complex mixtures using gas chromatography with unit-mass resolution electron ionization mass
484 spectrometry, *Anal. Chem.*, 92(18), 12481–12488, doi:10.1021/acs.analchem.0c02308, 2020.
- 485 Jaoui, M., Kleindienst, T. E., Lewandowski, M. and Edney, E. O.: Identification and quantification of aerosol polar
486 oxygenated compounds bearing carboxylic or hydroxyl groups. 1. Method development, *Anal. Chem.*, 76(16),
487 4765–4778, doi:10.1021/ac049919h, 2004.
- 488 Jaoui, M., Kleindienst, T. E., Lewandowski, M., Offenberg, J. H. and Edney, E. O.: Identification and quantification
489 of aerosol polar oxygenated compounds bearing carboxylic or hydroxyl groups. 2. Organic tracer compounds from
490 monoterpenes, *Environ. Sci. Technol.*, 39(15), 5661–5673, doi:10.1021/es048111b, 2005.
- 491 Kaltsonoudis, C., Kostenidou, E., Louvaris, E., Psichoudaki, M., Tsiligiannis, E., Florou, K., Liangou, A. and
492 Pandis, S. N.: Characterization of fresh and aged organic aerosol emissions from meat charbroiling, *Atmos. Chem.*
493 *Phys.*, 17(11), 7143–7155, doi:10.5194/acp-17-7143-2017, 2017.
- 494 Katragadda, H. R., Fullana, A., Sidhu, S. and Carbonell-Barrachina, A. A.: Emissions of volatile aldehydes from
495 heated cooking oils, *Food Chem.*, 120(1), 59–65, doi:10.1016/j.foodchem.2009.09.070, 2010.
- 496 Klein, F., Platt, S. M., Farren, N. J., Detournay, A., Bruns, E. A., Bozzetti, C., Daellenbach, K. R., Kilic, D., Kumar,
497 N. K., Pieber, S. M., Slowik, J. G., Temime-roussel, B., Marchand, N., Hamilton, J. F., Baltensperger, U., Prévôt, A.
498 S. H. and El Haddad, I.: Characterization of Gas-Phase Organics Using Proton Transfer Reaction Time-of-Flight

499 Mass Spectrometry: Cooking Emissions, *Environ. Sci. Technol.*, 50(3), 1243–1250, doi:10.1021/acs.est.5b04618,
500 2016a.

501 Klein, F., Farren, N. J., Bozzetti, C., Daellenbach, K. R., Kilic, D., Kumar, N. K., Pieber, S. M., Slowik, J. G.,
502 Tuthill, R. N., Hamilton, J. F., Baltensperger, U., Prévôt, A. S. H. and El Haddad, I.: Indoor terpene emissions from
503 cooking with herbs and pepper and their secondary organic aerosol production potential, *Sci. Rep.*, 6, 1–7,
504 doi:10.1038/srep36623, 2016b.

505 Klein, F., Baltensperger, U., Prévôt, A. S. H. and El Haddad, I.: Quantification of the impact of cooking processes
506 on indoor concentrations of volatile organic species and primary and secondary organic aerosols, *Indoor Air*, 29(6),
507 926–942, doi:10.1111/ina.12597, 2019.

508 Kostenidou, E., Florou, K., Kaltsonoudis, C., Tsiflikiotou, M., Vratolis, S., Eleftheriadis, K. and Pandis, S. N.:
509 Sources and chemical characterization of organic aerosol during the summer in the eastern Mediterranean, *Atmos.*
510 *Chem. Phys.*, 15(19), 11355–11371, doi:10.5194/acp-15-11355-2015, 2015.

511 Kroll, J. H., Donahue, N. M., Jimenez, J. L., Kessler, S. H., Canagaratna, M. R., Wilson, K. R., Altieri, K. E.,
512 Mazzoleni, L. R., Wozniak, A. S., Bluhm, H., Mysak, E. R., Smith, J. D., Kolb, C. E. and Worsnop, D. R.: Carbon
513 oxidation state as a metric for describing the chemistry of atmospheric organic aerosol, *Nat. Chem.*, 3(2), 133–139,
514 doi:10.1038/nchem.948, 2011.

515 Lee, B. P., Li, Y. J., Yu, J. Z., Louie, P. K. K. and Chan, C. K.: Characteristics of submicron particulate matter at the
516 urban roadside in downtown Hong Kong—overview of 4 months of continuous high-resolution aerosol mass
517 spectrometer measurements, *J. Geophys. Res.*, 120(14), 7040–7058, doi:10.1002/2015JD023311. Received, 2015.

518 Liu, T., Liu, Q., Li, Z., Huo, L., Chan, M. N., Li, X., Zhou, Z. and Chan, C. K.: Emission of volatile organic
519 compounds and production of secondary organic aerosol from stir-frying spices, *Sci. Total Environ.*, 599–600,
520 1614–1621, doi:10.1016/j.scitotenv.2017.05.147, 2017a.

521 Liu, T., Li, Z., Chan, M. and Chan, C. K.: Formation of secondary organic aerosols from gas-phase emissions of
522 heated cooking oils, *Atmos. Chem. Phys.*, 17(12), 7333–7344, doi:10.5194/acp-17-7333-2017, 2017b.

523 Liu, T., Wang, Z., Huang, D. D., Wang, X. and Chan, C. K.: Significant Production of Secondary Organic Aerosol
524 from Emissions of Heated Cooking Oils, *Environ. Sci. Technol. Lett.*, 5(1), 32–37, doi:10.1021/acs.estlett.7b00530,
525 2017c.

526 Liu, T., Wang, Z., Wang, X. and Chan, C. K.: Primary and secondary organic aerosol from heated cooking oil
527 emissions, *Atmos. Chem. Phys.*, 18(15), 11363–11374, doi:10.5194/acp-18-11363-2018, 2018.

528 Lopez-Hilfiker, F. D., Pospisilova, V., Huang, W., Kalberer, M., Mohr, C., Stefenelli, G., Thornton, J. A.,
529 Baltensperger, U., Prevot, A. S. H. and Slowik, J. G.: An Extractive Electrospray Ionization Time-of-Flight Mass
530 Spectrometer (EESI-TOF) for online measurement of atmospheric aerosol particles, *Atmos. Meas. Tech.*, 12(9), 1–
531 40, doi:10.5194/amt-2019-45, 2019.

532 Mao, J., Ren, X., Brune, W. H., Olson, J. R., Crawford, J. H., Fried, A., Huey, L. G., Cohen, R. C., Heikes, B.,
533 Singh, H. B., Blake, D. R., Sachse, G. W., Diskin, G. S., Hall, S. R. and Shetter, R. E.: Airborne measurement of
534 OH reactivity during INTEX-B, *Atmos. Chem. Phys.*, 9(1), 163–173, doi:10.5194/acp-9-163-2009, 2009.

535 McDonald, B. C., De Gouw, J. A., Gilman, J. B., Jathar, S. H., Akherati, A., Cappa, C. D., Jimenez, J. L., Lee-
536 Taylor, J., Hayes, P. L., McKeen, S. A., Cui, Y. Y., Kim, S. W., Gentner, D. R., Isaacman-VanWertz, G., Goldstein,
537 A. H., Harley, R. A. and Frost, M.: Volatile chemical products emerging as largest petrochemical source of urban
538 organic emissions, *Science* (80-.), 359(6377), 760–764, doi:10.1126/science.aaq0524, 2018.

539 Mohr, C., Huffman, J. A., Cubison, M. J., Aiken, A. C., Docherty, K. S., Kimmel, J. R., Ulbrich, I. M., Hannigan,
540 M. and Jimenez, J. L.: Characterization of primary organic aerosol emissions from meat cooking, trash burning, and
541 motor vehicles with high-resolution aerosol mass spectrometry and comparison with ambient and chamber
542 observations, *Environ. Sci. Technol.*, 43(7), 2443–2449, doi:10.1021/es8011518, 2009.

543 Mohr, C., Decarlo, P. F., Heringa, M. F., Chirico, R., Slowik, J. G., Richter, R., Reche, C., Alastuey, A., Querol, X.,
544 Seco, R., Penuelas, J., Jimenez, J. L., Crippa, M., Zimmermann, R., Baltensperger, U. and Prévôt, A. S. H.:
545 Identification and quantification of organic aerosol from cooking and other sources in Barcelona using aerosol mass
546 spectrometer data, *Atmos. Chem. Phys.*, 12(4), 1649–1665, doi:10.5194/acp-12-1649-2012, 2012.

547 Pankow, J. F. and Asher, W. E.: SIMPOL.1: A simple group contribution method for predicting vapor pressures and
548 enthalpies of vaporization of multifunctional organic compounds, *Atmos. Chem. Phys.*, 8(10), 2773–2796,
549 doi:10.5194/acp-8-2773-2008, 2008.

550 Riipinen, I., Pierce, J. R., Donahue, N. M. and Pandis, S. N.: Equilibration time scales of organic aerosol inside
551 thermodenuders: Evaporation kinetics versus thermodynamics, *Atmos. Environ.*, 44(5), 597–607,
552 doi:10.1016/j.atmosenv.2009.11.022, 2010.

553 Rothfuss, N. E. and Petters, M. D.: Influence of functional groups on the viscosity of organic aerosol, *Environ. Sci.*
554 *Technol.*, 51(1), 271–279, doi:10.1021/acs.est.6b04478, 2016.

555 Schauer, J. J., Kleeman, M. J., Cass, G. R. and Simoneit, B. R. T.: Measurement of emissions from air pollution
556 sources. 1. C1 through C29 organic compounds from meat charbroiling, *Environ. Sci. Technol.*, 33(10), 1566–1577,
557 doi:10.1021/es980076j, 1999.

558 Schauer, J. J., Kleeman, M. J., Cass, G. R. and Simoneit, B. R. T.: Measurement of emissions from air pollution
559 sources. 4. C1-C27 organic compounds from cooking with seed oils, *Environ. Sci. Technol.*, 36(4), 567–575,
560 doi:10.1021/es002053m, 2002.

561 Shiraiwa, M., Zuend, A., Bertram, A. K. and Seinfeld, J. H.: Gas-particle partitioning of atmospheric aerosols:
562 Interplay of physical state, non-ideal mixing and morphology, *Phys. Chem. Chem. Phys.*, 15(27), 11441–11453,
563 doi:10.1039/c3cp51595h, 2013.

564 Sun, Y.-L., Zhang, Q., Schwab, J. J., Demerjian, K. L., Chen, W.-N., Bae, M.-S., Hung, H.-M., Hogrefe, O., Frank,
565 B., Rattigan, O. V. and Lin, Y.-C.: Characterization of the sources and processes of organic and inorganic aerosols
566 in New York city with a high-resolution time-of-flight aerosol mass spectrometer, *Atmos. Chem. Phys.*, 11(4),
567 1581–1602, doi:10.5194/acp-11-1581-2011, 2011.

568 Takhar, M., Stroud, C. A. and Chan, A. W. H.: Volatility Distribution and Evaporation Rates of Organic Aerosol
569 from Cooking Oils and their Evolution upon Heterogeneous Oxidation, *ACS Earth Sp. Chem.*, 3(9), 1717–1728,
570 doi:10.1021/acsearthspacechem.9b00110, 2019.

571 Ye, J., Gordon, C. A. and Chan, A. W. H.: Enhancement in Secondary Organic Aerosol Formation in the Presence
572 of Preexisting Organic Particle, *Environ. Sci. Technol.*, 50(7), 3572–3579, doi:10.1021/acs.est.5b05512, 2016.

573 Ye, J., Van Rooy, P., Adam, C. H., Jeong, C. H., Urch, B., Cocker, D. R., Evans, G. J. and Chan, A. W. H.:
574 Predicting Secondary Organic Aerosol Enhancement in the Presence of Atmospherically Relevant Organic Particles,
575 *ACS Earth Sp. Chem.*, 2(10), 1035–1046, doi:10.1021/acsearthspacechem.8b00093, 2018.

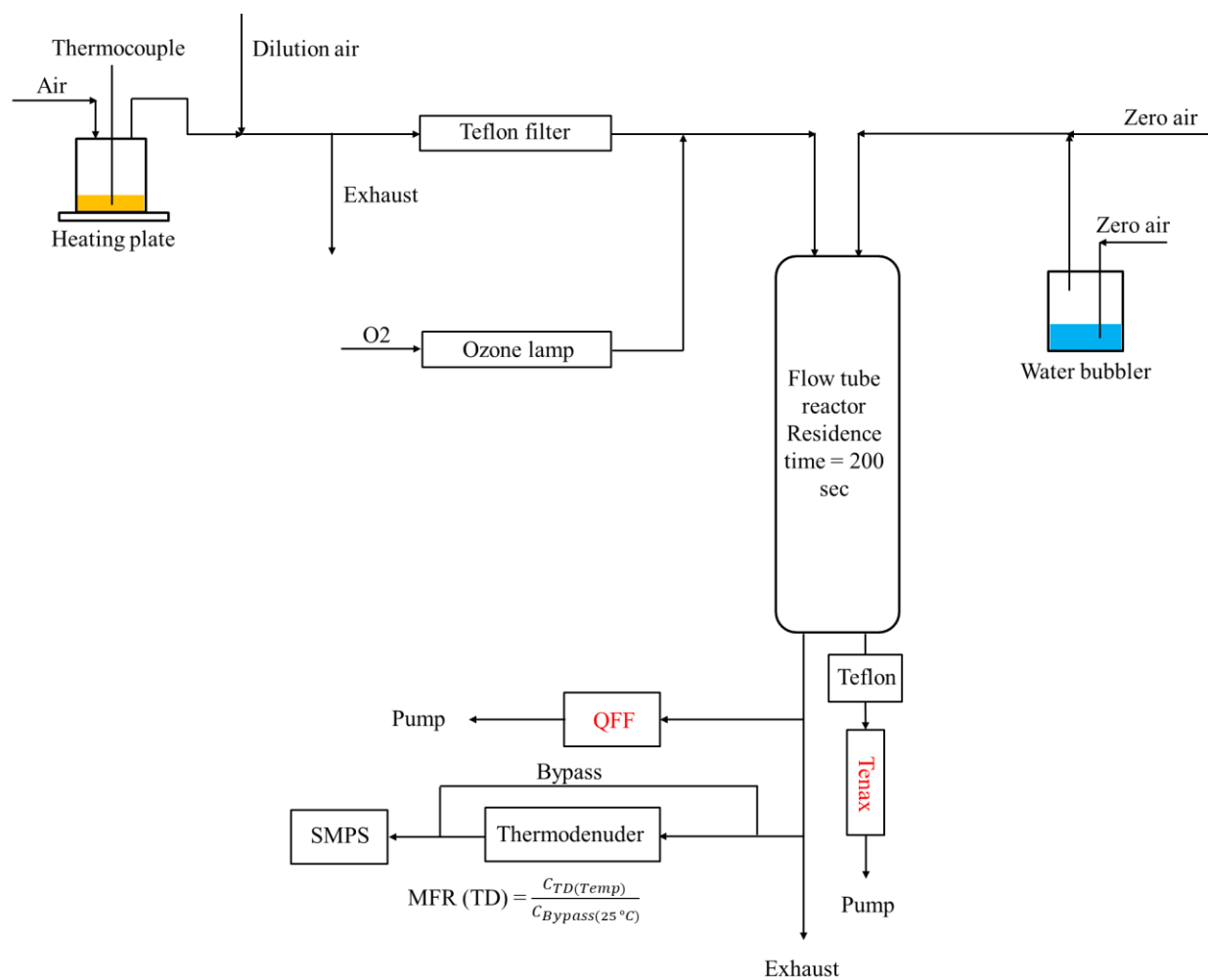
576 Yu, J., Flagan, R. C. and Seinfeld, J. H.: Identification of products containing -COOH, -OH, and -C=O in
577 atmospheric oxidation of hydrocarbons, *Environ. Sci. Technol.*, 32(16), 2357–2370, doi:10.1021/es980129x, 1998.

578 Zhao, Y., Hennigan, C. J., May, A. A., Tkacik, D. S., De Gouw, J. A., Gilman, J. B., Kuster, W. C., Borbon, A. and
579 Robinson, A. L.: Intermediate-volatility organic compounds: A large source of secondary organic aerosol, *Environ.*
580 *Sci. Technol.*, 48(23), 13743–13750, doi:10.1021/es5035188, 2014.

581 Zhao, Y., Nguyen, N. T., Presto, A. A., Hennigan, C. J., May, A. A. and Robinson, A. L.: Intermediate Volatility
582 Organic Compound Emissions from On-Road Diesel Vehicles: Chemical Composition, Emission Factors, and
583 Estimated Secondary Organic Aerosol Production, *Environ. Sci. Technol.*, 49(19), 11516–11526,
584 doi:10.1021/acs.est.5b02841, 2015.

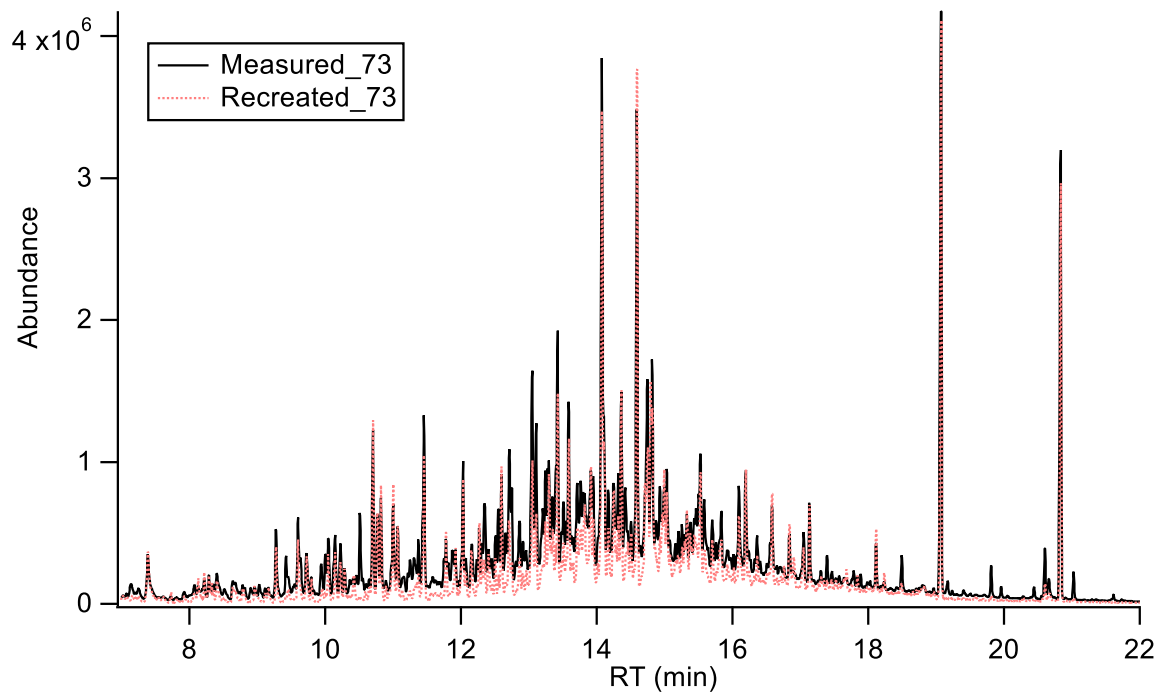
585 Zuend, A. and Seinfeld, J. H.: Modeling the gas-particle partitioning of secondary organic aerosol: The importance
586 of liquid-liquid phase separation, *Atmos. Chem. Phys.*, 12(9), 3857–3882, doi:10.5194/acp-12-3857-2012, 2012.

587



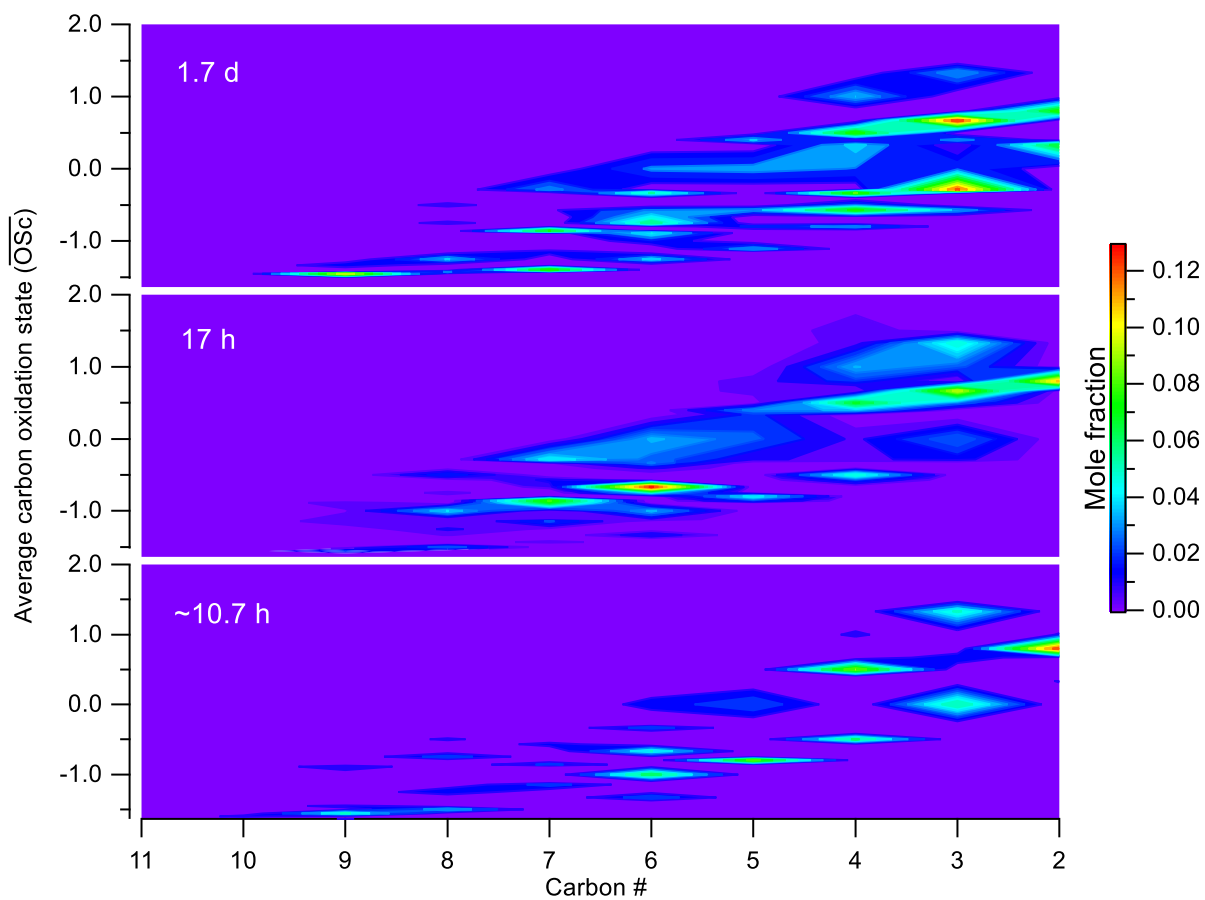
588

589 **Figure 1.** Experimental setup for oxidation of heated cooking oil emissions.



590

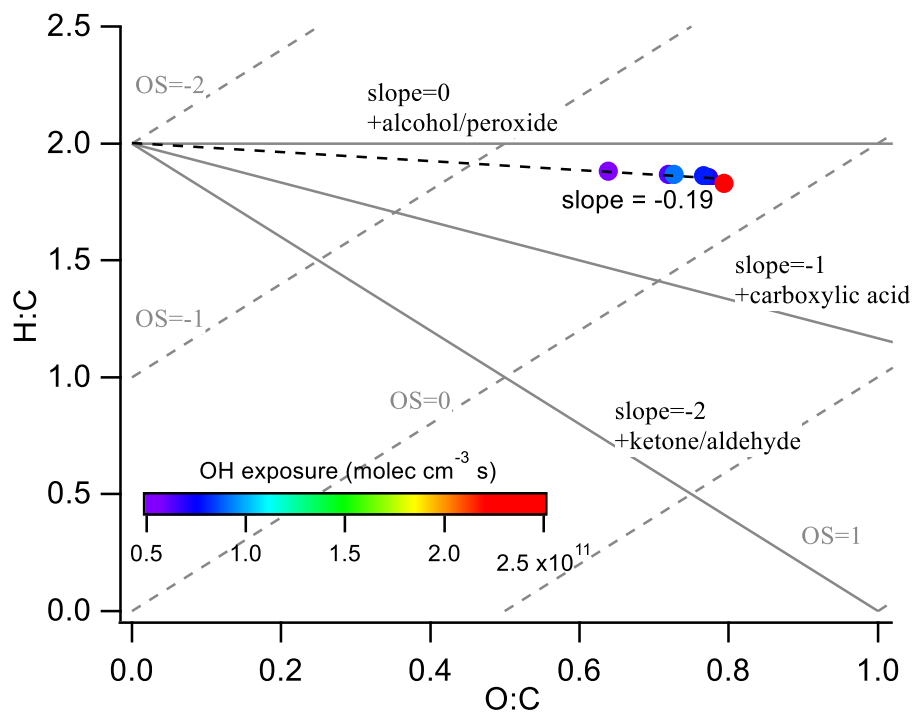
591 **Figure 2.** Highly complex mixture of canola oil SOA generated upon photooxidation. With known signal and mass fragmentation,
592 signal of m/z 73 can be recreated based on pseudo parent ions (e.g. M-15 used in this study).



593

594 **Figure 3.** Evolution in \overline{OSc} -nc space for canola oil SOA under different conditions of photochemical aging. As the oxidation
 595 progresses in the atmosphere, more compounds are formed with smaller nc and higher \overline{OSc} suggesting fragmentation to be a
 596 dominant pathway of oxidation for cooking emissions in the atmosphere.

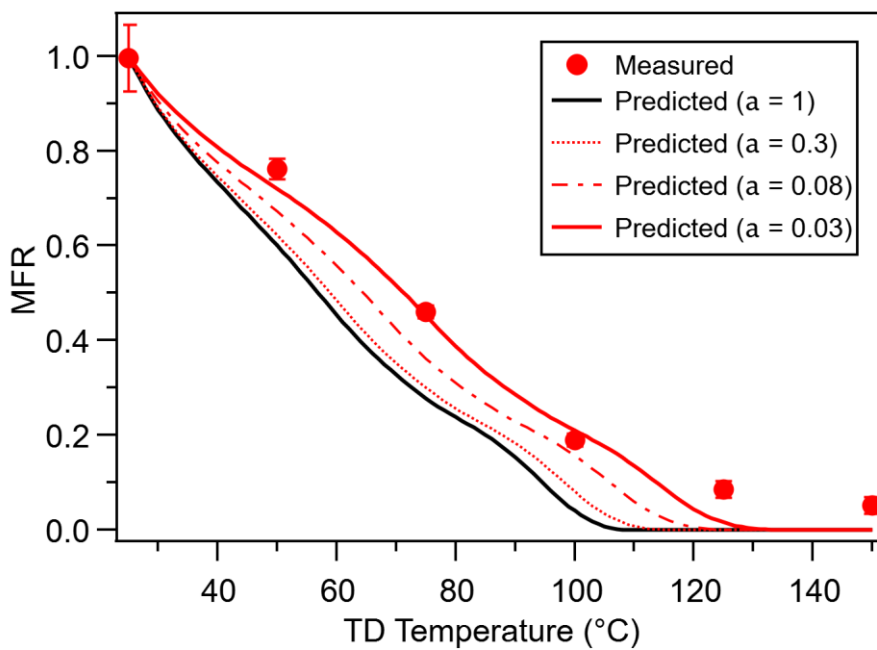
597



598

599 **Figure 4.** Van Krevelen diagram of canola oil SOA coloured by different OH exposure. In the background, average carbon
 600 oxidation state (\overline{OS}_c) and functionalization slopes are shown for reference. The slope of -0.19 for canola oil SOA corresponds to
 601 formation of both alcohol and carboxylic acid consistent with the chemical composition obtained from TD-GC/MS.

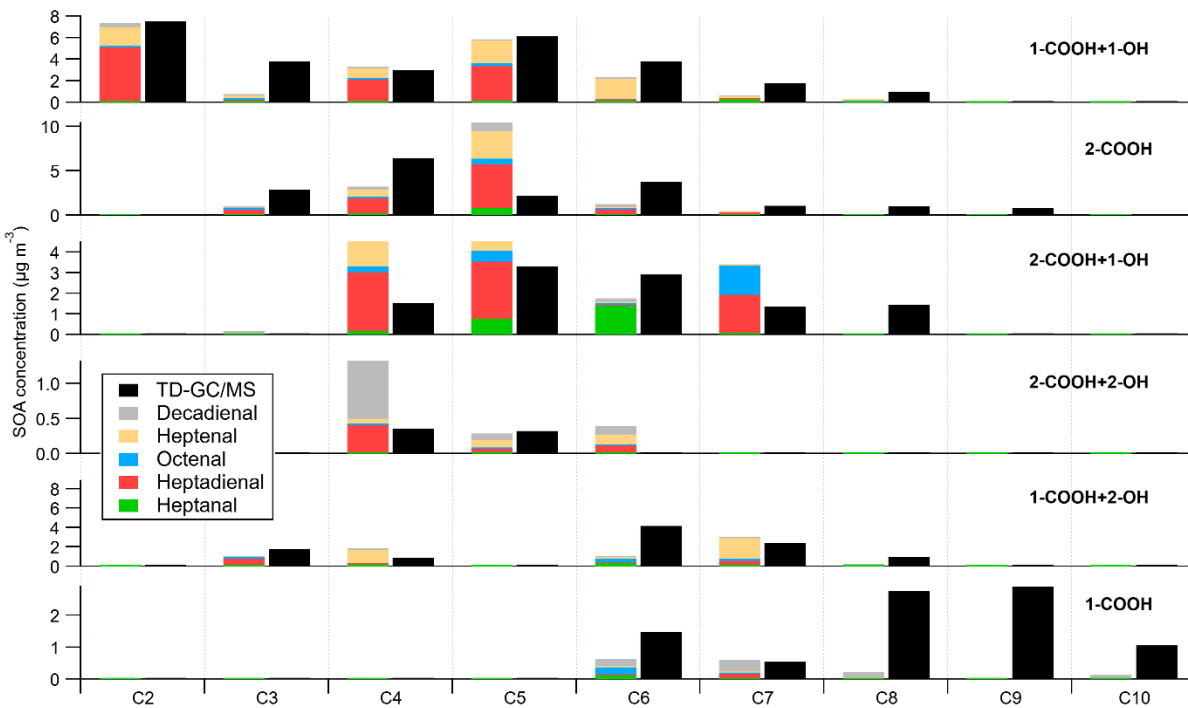
602



603

604 **Figure 5.** Mass thermogram of canola oil SOA at an OH exposure of 9.23×10^{10} molecules cm^{-3} s. The black line represents model
605 simulations using $\alpha = 1$ underpredicting the measured MFR. The red line corresponds to model simulations using $\alpha = 0.03$ predicting
606 the measurements reasonably well, therefore implying kinetic limitations in the system. The error bars represent $\pm 1\sigma$.

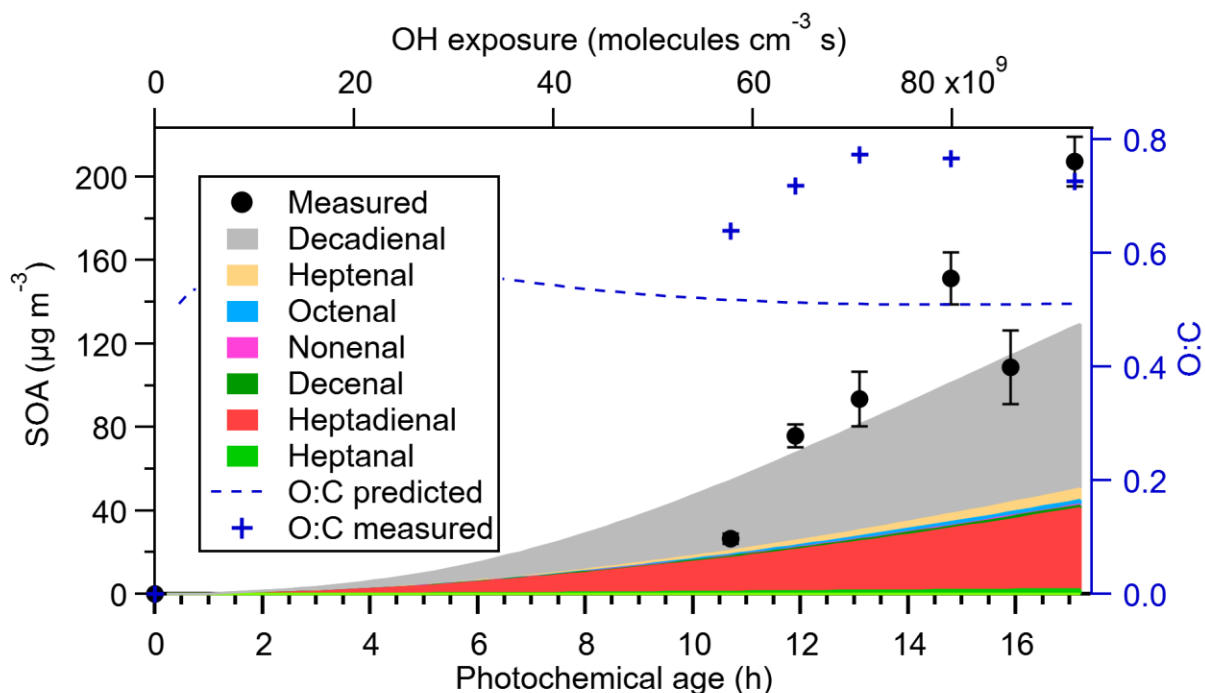
607



608

609 **Figure 6.** Prediction of different compounds formed at an OH exposure of 6.43×10^{10} molecules cm^{-3} s using product molar yields
 610 of heptanal, heptenal, octenal, heptadienal, and decadienal. The total aldehydes products can explain the observed oil SOA products
 611 within a factor of half, while the inconsistency in prediction of some SOA products is likely caused by differences in gas-particle
 612 partitioning in both photooxidation systems.

613



614
 615 **Figure 7.** SOM prediction of SOA produced from different aldehydes with increasing photochemical age. The model overpredicts
 616 SOA formation at lower photochemical age, while underpredicts SOA formation by ~40% at higher photochemical age, suggesting
 617 that traditional VOC precursors cannot fully explain the SOA formation, and other gas-phase precursors maybe needed to better
 618 constrain the formation of SOA at higher aging conditions. In addition, the SOM predicted O:C is within 50% of the measured O:C
 619 suggesting that the overall change in chemical composition of cooking SOA is predicted reasonably well.